JOM, Vol. 76, No. 3, 2024
https://doi.org/10.1007/s11837-023-06342-z

Investigation into the Impact of Fe_2O_3, MgO, and Al_2O_3 Contents on the Ca Ions Leaching Rate of Steel Slag

YINBO LUO ,[1,3] DONGFENG HE,[2] and GELE QING[1]

1.—Shougang Research Institute of Technology, Shougang Group, Beijing 100043, China. 2.—School of Metallurgical and Ecological Engineering, University of Science and Technology Beijing, Beijing 100083, China. 3.—e-mail: luoyb@shougang.com.cn

Indirect carbonation, as an effective technique for CO_2 sequestration, has gained widespread attention in today's society due to the increasing severity of the greenhouse effect. The present study proposed a strategy to enhance the CO_2 sequestration capacity of steel slag by increasing the content of Ca_2SiO_4 with highly reactive activity through high-temperature modification. The research focused on investigating the impact of major chemical components of steel slag on the Ca ions leaching rate. The results indicated that, as the Fe_2O_3 content decreases, the formation of Ca_2SiO_4 becomes more favorable. When the Fe_2O_3 content was reduced from 30 wt.% to 15 wt.%, the Ca ions leaching rate increased from 92.01% to 98.26%. The presence of MgO and Al_2O_3 in steel slag can reduce the content of Ca_2SiO_4, which has a negative impact on the Ca ions leaching rate. Additionally, the mineral composition of the leaching residue consists predominantly of iron-rich minerals, such as spinel and RO phase. Overall, the modification–leaching process enables the effective extraction and recovery of valuable metal elements from steel slag, which is highly significant for the resource utilization of solid waste.

INTRODUCTION

The gradual increase in atmospheric CO_2 concentration and the subsequent cascade of ecological and environmental issues are increasingly impacting the sustainable development of human society.[1] Concerns about CO_2-related issues arise as we witness the melting of ice caps, rising of sea levels, and frequent natural disasters, among other problems.[2] The atmospheric concentration of CO_2 has increased from 280 ppm before the Industrial Revolution to the current level of 422 ppm,[3] representing a growth of 50.71%. It is imperative for human society to take effective measures to reduce CO_2 emissions as a pressing issue.

Mineral carbonation technology is considered an effective means of reducing CO_2 emissions and has received increasing attention in recent years.[4–12] Mineral carbonation is an accelerated process that mimics the natural weathering of rocks, where CO_2 is captured and fixed into minerals. It involves the reaction of alkaline earth metal elements present in rock minerals with CO_2 to form thermodynamically stable carbonates.[13,14] Steel slag, due to its high Ca content, is an ideal raw material for mineral carbonation.[15]

The iron and steel industry serves as both the source of steel slag generation and of CO_2 emissions.[16,17] Utilizing steel slag as a raw material for carbonation reactions can leverage its high calcium content to react with CO_2, achieving the purpose of CO_2 fixation.[18] Additionally, the carbonation of steel slag can also achieve the purpose of treating waste with waste. Steel slag carbonation can be divided into direct carbonation and indirect carbonation.[19,20] Direct carbonation refers to the process by which steel slag reacts with CO_2 in a single step to produce carbonates.[21–23] Indirect carbonation, on the other hand, involves two steps, leaching and carbonation:[24,25] (1) in the leaching step, steel slag is subjected to wet extraction to obtain a calcium-rich leachate; and (2) subsequently, CO_2 is introduced into the leachate to initiate the carbonation precipitation reaction. Indirect carbonation is

(Received September 11, 2023; accepted December 6, 2023; published online December 29, 2023)

widely studied due to its high carbonation rate and the potential to generate high-value by-products such as precipitated calcium carbonate.

The primary mineral components of steel slag are Ca_2SiO_4 (C_2S) and $Ca_2Fe_2O_5$ (C_2F). Su et al.'s research confirmed this finding. They found that the calcium-bearing mineral phases present in steel slag include f-CaO (5–10%), calcium silicate phase (~ 40%), and calcium ferrite phase (~ 30%).[26] In other words, the Ca elements in steel slag are primarily distributed within C_2S and C_2F. Indeed, C_2S exhibits higher reactivity and readily contributes Ca elements to participate in carbonation reactions.[27] On the other hand, C_2F has a lower reactivity, making it challenging to extract Ca elements from it.[28] This results in the underutilization of Ca elements in steel slag for carbonation reactions. In other words, the Ca ions leaching rate (CLR) of steel slag is low, and a low CLR indicates a lesser amount of raw material available for the carbonation reaction, resulting in a decreased capacity for CO_2 fixation by steel slag. Therefore, improving the CLR of steel slag is the key to its indirect carbonation process.

Regarding the relationship between mineral phases and leaching efficiency, the research conducted by Lee et al. demonstrated that the extraction efficiency of Ca element from steel slag is significantly influenced by the mineral composition of the slag.[29] In the study conducted by Zhao et al., chemical reagents were utilized to synthesize the pure mineral phases found in steel slag, followed by leaching experiments. The results indicated the following order of leaching efficiency for Ca ions: CaO > γ-C_2S > $Ca_3Mg(SiO_4)_2$ (C_3MS_2) > $Ca_2MgSi_2O_7$ (C_2MS_2) > $Ca_2Al_2SiO_7$ (C_2AS).[30] In another study conducted by Zhao et al.,[31] the same method was employed to synthesize additional calcium-containing mineral phases, such as $CaAl_2O_4$ (CA), $Ca_3Al_2O_6$ (C_3A), $Ca_{12}Al_{14}O_{33}$ ($C_{12}A_7$), and C_2F, among others. The results of the leaching reaction indicated that CaO exhibited the highest leaching ability in an acidic environment, followed by C_3A and silicate minerals. On the other hand, $C_{12}A_7$, CA, and C_2F showed the lowest leaching ability for the Ca element. In our previous study,[32] thermodynamic calculations were performed to determine the Gibbs free energy (ΔG) of reactions between various minerals in steel slag and acetic acid. The results revealed that the ΔG of reaction for each mineral with acetic acid follows the order: Ca_3SiO_5 (C_3S) > C_3MS_2 > C_2S > C_2MS_2 > C_2AS > C_2F > $Ca_3Fe_2Si_3O_{12}$ (C_3FS_3) > $MgFe_2O_4$ > Fe_3O_4. Subsequently, high-temperature modification experiments were conducted on the steel slag by adding SiO_2. The experimental results indicated that, in high-alkaline steel slag, the mineral composition consisted of C_2F and C_2S. With an basicity of 4, the CLR of the modified slag was only 62.00%. As the basicity decreased, the CLR gradually increased. At an basicity of 2, the main mineral phases in the slag were C_2S and C_3MS_2, resulting in the highest CLR of 84.46% of the modified slag. Further reducing the basicity to 1 led to the main mineral composition of the slag being $Ca_3Fe_2Si_3O_{12}$ and C_3MS_2, resulting in a significant decrease in the CLR to only 61.04%.

In response to the overall low Ca element extraction efficiency of steel slag, a method of high-temperature modification to alter the mineral composition of steel slag so as to enhance its CLR has been proposed. Specifically, by adding silica-based materials to steel slag and subjecting them to high-temperature modification, the C_2F of the slag is transformed into C_2S and iron-rich phases (such as spinel and the RO phase). As a result, the Ca element in steel slag is predominantly distributed within the highly reactive C_2S phase, which significantly enhances the CLR of the slag. In addition, the Fe element is separated from C_2F and exists within structurally stable iron-rich phases, and is retained in the leaching residue after the leaching reaction.

In our previous research, the effects of basicity and calcination temperature on the mineral composition and the CLR of steel slag were investigated through modification experiments. The experimental results indicate that at an basicity level of 2 and a calcination temperature of 1500°C, the CLR of the modified slag reached 94.62%, which is a significant improvement compared to the CLR of 59.28% observed in the original steel slag. On this basis, this study further investigated the impact of variations in the content of other major chemical components, namely Fe_2O_3, MgO, and Al_2O_3, in steel slag on the mineral composition of the slag and the CLR. The experiments have been conducted under specific conditions, including a basicity of 2 and a calcination temperature of 1500°C. The objective is to establish an understanding of the relationship between the CLR of steel slag and the content of its primary chemical components, which will serve as a reference for predicting and optimizing the leaching reactions of steel slag with different components. Overall, the modification–leaching process enables the effective extraction of valuable metal elements (such as Ca and Fe) from steel slag, which has significant implications for the resource utilization of steel slag.

MATERIALS AND METHODS

Materials

The steel slag utilized in the experiment was sourced from a steel mill. Prior to the high-temperature modification test, the steel slag underwent a series of preparation steps. Firstly, it was dried at 105°C in a drying oven for 24 h to eliminate moisture. Subsequently, the dried steel slag was crushed and screened, and only the portion passing through a 200-mesh square hole sieve was selected for the test. The chemical composition of the steel slag was analyzed using X-ray fluorescence (XRF;

Shimadzu XRF-1800) testing, and the corresponding results are presented in Table I. The SiO_2 (>99.5 wt.%, AR) used in the experiment was purchased from Sinopharm Chemical Reagent Beijing; CaO (> 98 wt.%, AR), Fe_2O_3 (> 99 wt.%, AR), Al_2O_3 (> 99 wt.%, AR) were purchased from Shanghai McLean Biochemical Technology; MgO (> 98.5 wt.%, AR) was purchased from Shanghai Yuanye Bio-Technology; nitrogen gas (> 99.5 wt.%) was purchased from Beijing Prax Practical Gas; and CH_3COOH (> 99.5 wt.%, AR) was purchased from Saen Chemical Technology, Shanghai.

Methods

Thermal Modification Experiment

Based on previous studies, it has been established that the CLR of modified slag reached its maximum when the basicity was set at 2. Therefore, for each group of modified slag in this study, the basicity was deliberately set at 2 to ensure consistency and comparability with the previous findings. This paper focuses on investigating the influence of the Fe_2O_3, MgO, and Al_2O_3 contents on the mineral composition as well as the CLR of the modified slag. The objective is to understand how variations in these specific components impact the overall characteristics and performance of the modified slag. To achieve the desired composition, chemical reagents such as CaO, SiO_2, Fe_2O_3, MgO, and Al_2O_3 were introduced and added to the steel slag. The addition of these reagents was carefully controlled to ensure that each main component reaches the predetermined target value. This precise adjustment of the composition allows for systematic investigations and analysis of the modified slag's properties and performance. In this study, the mass fractions of Fe_2O_3 were deliberately set at 30 wt.%, 25 wt.%, 20 wt.%, and 15 wt.%. Similarly, the mass fractions of MgO were varied as 3 wt.%, 6 wt.%, 9 wt.%, and 12 wt.%. Additionally, the mass fractions of Al_2O_3 were adjusted to 3 wt.%, 6 wt.%, 9 wt.%, and 12 wt.%. The quantities of materials added to each modified slag sample are presented in Table II, while the corresponding chemical compositions are presented in Table III. The steel slag and chemical reagents were thoroughly mixed using a ball mill to ensure homogeneity. Subsequently, the resulting mixture was loosely loaded into a MgO crucible. The crucible, containing the mixture, was then placed inside a Si-Mo tubular electric furnace. The tube furnace was purged with N_2 at a flow rate of 1 L/min to create an inert atmosphere. The temperature of the furnace was then gradually increased to 1500°C at a heating rate of 5°C/min. Once the desired temperature was reached, it was maintained for a duration of 30 min to ensure complete high-temperature treatment of the modified slag. After the firing process, the modified slag samples were carefully taken out from the furnace and placed in ambient air for natural cooling. In the final step, the modified slag was fractured, and a small number of bulk samples were extracted for further analysis. These samples were prepared by creating mosaics, followed by grinding and polishing, and were then subjected to scanning electron microscopy with backscattered electron detector (SEM-BSD) (ZEISS EVO18) observation. At the same time, an EDS electron probe (Ultim Msx 170) was used to analyze the components of the different microphases during the SEM observations. The remaining modified slag was crushed using a crusher for a duration of 60 s.

Table I. Chemical composition of original steel slag

Constituent	CaO	SiO_2	Fe_2O_3	MgO	Al_2O_3	P_2O_5	MnO	TiO_2	V_2O_5	Cr_2O_3	Others
Contents (wt.%)	46.70	10.68	29.50	4.81	0.97	2.28	2.35	1.34	0.81	0.32	0.24

Table II. The raw material addition amount of different modified slag

	Content/ wt.%	Steel slag/g	CaO/g	SiO_2/g	Fe_2O_3/g	MgO/g	Al_2O_3/g
Fe_2O_3 modified slag	30	40.68	0.35	5.33	3.00	0.54	0.10
	25	42.37	1.14	5.94	–	0.46	0.09
	20	33.90	7.18	7.88	–	0.87	0.17
	15	25.42	13.22	9.83	–	1.28	0.25
MgO modified slag	3	30.51	7.93	7.83	3.50	0.03	0.20
	6	30.51	6.93	7.33	3.50	1.53	0.20
	9	30.51	5.93	6.83	3.50	3.03	0.20
	12	30.51	4.93	6.33	3.50	4.53	0.20
Al_2O_3 modified slag	3	30.51	7.26	7.50	3.50	0.03	1.20
	6	30.51	6.26	7.00	3.50	0.03	2.70
	9	30.51	5.26	6.50	3.50	0.03	4.20
	12	30.51	4.26	6.00	3.50	0.03	5.70

Table III. Chemical composition of different modified slag

	Content/ wt.%	CaO/ wt.%	SiO_2/ wt.%	Fe_2O_3/ wt.%	MgO/ wt.%	Al_2O_3/ wt.%	P_2O_5/ wt.%	MnO/ wt.%	TiO_2/ wt.%	V_2O_5/ wt.%	Others/ wt.%
Fe_2O_3	30	38.68	19.34	30.00	5.00	1.00	1.86	1.91	1.09	0.66	0.46
modified	25	41.85	20.93	25.00	5.00	1.00	1.93	1.99	1.14	0.68	0.49
slag	20	46.01	23.01	20.00	5.00	1.00	1.55	1.59	0.91	0.55	0.39
	15	50.18	25.09	15.00	5.00	1.00	1.16	1.19	0.68	0.41	0.29
MgO	3	44.35	22.18	25.00	3.00	1.00	1.39	1.43	0.82	0.49	0.35
modified	6	42.35	21.18	25.00	6.00	1.00	1.39	1.43	0.82	0.49	0.35
slag	9	40.35	20.18	25.00	9.00	1.00	1.39	1.43	0.82	0.49	0.35
	12	38.35	19.18	25.00	12.00	1.00	1.39	1.43	0.82	0.49	0.35
Al_2O_3	3	43.01	21.51	25.00	3.00	3.00	1.39	1.43	0.82	0.49	0.35
modified	6	41.01	20.51	25.00	3.00	6.00	1.39	1.43	0.82	0.49	0.35
slag	9	39.01	19.51	25.00	3.00	9.00	1.39	1.43	0.82	0.49	0.35
	12	37.01	18.51	25.00	3.00	12.00	1.39	1.43	0.82	0.49	0.35

The crushed slag was ground in a ball mill at a speed of 500 rpm for 15 min, and the resulting ground material was then sieved through a 300-mesh square hole screen. The fraction passing through the screen was reserved for the leaching experiment. Additionally, a small quantity of the powdered sample was extracted for X-ray diffraction (XRD; Rigaku D/max 2500) analysis.

The Fe_2O_3 modified slag samples were numbered as FC30, FC25, FC20, and FC15; the MgO modified slag samples were numbered as MC3, MC6, MC9, and MC12; and the Al_2O_3 modified slag samples were numbered as AC3, AC6, AC9, and AC12.

Leaching Experiment

A three-necked flask was placed in a magnetic water bath, and the temperature was set to 25 °C. Next, a 100-mL solution of 1 M CH_3COOH was prepared and added to the flask. A weight of 5 g of the slag was measured, and, once the set temperature of the CH_3COOH solution was reached, the slag was added to the three-necked flask and simultaneously the leaching reaction was initiated. The RS of the water bath was set to 500 rpm, and the reaction proceeded for a duration of 30 min. Following the completion of the leaching reaction, the reaction slurry was subjected to filtration using a vacuum filtration device, yielding a leachate and a leaching residue. The leachate underwent a dilution of 200 times, and the concentration of Ca ions was subsequently measured using inductively coupled plasma–optical emission spectrometry (Optima 7000 DV). Simultaneously, the pH of the leachate was determined using a pH meter. The leaching residue was dried in a drying oven and subjected to XRD analysis. The experimental flow chart of this research is shown in Fig. S1 (see online supplemental material), and the chemical reactions involved in the leaching reaction are as follows:

$$Ca_2SiO_4 + 4CH_3COOH = 2Ca^{2+} + 4CH_3COO^- + SiO_2 + 2H_2O \quad (1)$$

$$CaFe_2O_4 + 8CH_3COOH = Ca^{2+} + 2Fe^{3+} + 8CH_3COO^- + 4H_2O \quad (2)$$

$$Ca_2Fe_2O_5 + 10CH_3COOH = 2Ca^{2+} + 2Fe^{3+} + 10CH_3COO^- + 5H_2O \quad (3)$$

$$MgFe_2O_4 + 8CH_3COOH = Mg^{2+} + 2Fe^{3+} + 8CH_3COO^- + 4H_2O \quad (4)$$

$$Fe_3O_4 + 8CH_3COOH = Fe^{2+} + 2Fe^{3+} + 8CH_3COO^- + 4H_2O \quad (5)$$

$$FeO + 2CH_3COOH = Fe^{2+} + 2CH_3COO^- + H_2O \quad (6)$$

$$MgO + 2CH_3COOH = Mg^{2+} + 2CH_3COO^- + H_2O \quad (7)$$

$$Ca_3Mg(SiO_4)_2 + 8CH_3COOH = 3Ca^{2+} + Mg^{2+} + 8CH_3COO^- + 2SiO_2 + 4H_2O \quad (8)$$

The CLR of steel slag can be determined using Eq. 9, where C_{Ca} (mg/L) represents the concentration of Ca ions in the leachate, V (L) denotes the volume of the leachate, m_{slag} (g) represents the mass of the steel slag involved in the leaching reaction, and x_{Ca} (wt.%) indicates the mass fraction of Ca in the slag. x_{Ca} (wt.%) can be calculated by Eq. 10, where x_{CaO} (wt.%) denotes the mass fraction of steel slag, 40 is the relative atomic mass of the Ca, and 56 is the relative molecular mass of CaO:

$$\eta_{Ca} = \frac{C_{Ca} \cdot V}{m_{slag} \cdot x_{Ca}} \times \frac{1}{1000} \quad (9)$$

$$x_{Ca} = \frac{x_{CaO} \times 40}{56} \quad (10)$$

Thermodynamic Calculation

The thermodynamic calculations for determining the phase content changes during the solidification of modified slag were conducted using Factsage 7.1 software.[33,34] The main parameters of thermodynamic calculation were set as follows: the temperature interval was 50–1800°C, the step was 50°C, the pressure was 101.3 kPa, and the partial pressure of oxygen was 21.3 kpa. FToxid-SLAGA, FToxid-SPINA, FToxid-MeO_A, FToxid-bC_2SA, FToxid-aC_2SA, and FToxid-Mel_A were selected as the databases. The input components were CaO, SiO_2, Fe_2O_3, MgO, and Al_2O_3. The normalized data are shown in Table S1.

The viscosity of different modified slags at 1500°C was calculated using Factsage 7.1.

RESULTS AND DISCUSSION

Influence of Fe_2O_3 Content on Mineral Composition and CLR of Steel Slag

Thermodynamic Analysis

Figure 1 presents the thermodynamic calculation results for the modified slag with different Fe_2O_3 contents. During the cooling process of the modified slag, α-C_2S initially precipitated from the liquid phase. However, its content started to decrease at temperatures ranging from 1400 to 1450°C. Simultaneously, α′-C_2S began to precipitate in larger quantities and reached its peak concentration at temperatures between 1250 and 1350°C. Around

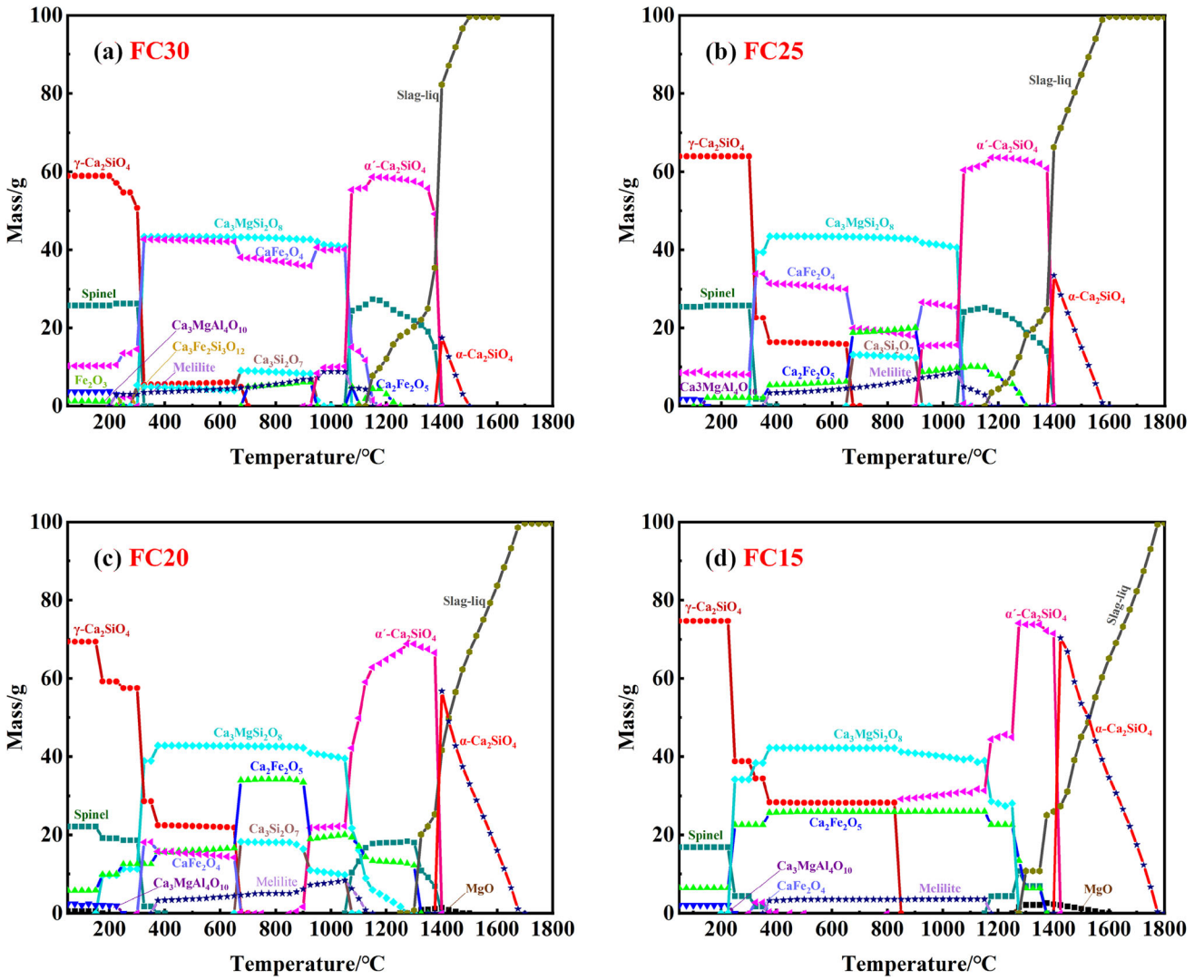

Fig. 1. Thermodynamic calculation results of modified slag with different Fe_2O_3 contents: (a) thermodynamic calculation results of FC30 modified slag; (b) thermodynamic calculation results of FC25 modified slag; (c) thermodynamic calculation results of FC20 modified slag; (d) thermodynamic calculation results of FC15 modified slag.

1100°C, the content of α'-C_2S starts to decline, while C_3MS_2 began to be continuously generated in the modified slag during the cooling process. In the temperature range of 350–1050°C, C_3MS_2 became the predominant silicate mineral in the modified slag. At approximately 700°C, the formation of γ-C_2S began in the modified slag during the cooling process. As the content of C_3MS_2 decreased, the proportion of γ-C_2S gradually increased. By the time the slag reached room temperature, γ-C_2S became the predominant silicate mineral. Ferrite minerals, namely C_2F and $CaFe_2O_4$ (CF), initiate precipitation within the temperature range of 1100–1350°C. Furthermore, within the temperature range of 350–1050°C, they became the predominant iron-bearing minerals in the modified slag. In the temperature range of 1050–1400°C and below 400°C, a higher amount of the spinel phase precipitated in the modified slag. As the slag cooled to room temperature, the main iron-bearing minerals identified were the spinel phase. Additionally, during the cooling process of the modified slag, minerals such as melilite and $Ca_3Si_2O_7$ were formed. For the modified slag with varying Fe_2O_3 contents, it was observed that, as the Fe_2O_3 content decreased, the content of γ-C_2S in the slag gradually increased. Conversely, the content of the spinel phase gradually decreased, when the slag was cooled to room temperature. Precisely, a decrease in Fe_2O_3 content in the modified slag leads to an enrichment of Ca elements in the silicate mineral γ-C_2S. This enrichment of Ca elements in γ-C_2S was beneficial for the extraction of Ca elements.

Influence of Fe_2O_3 Content on Mineral Composition of Steel Slag

The XRD patterns of the modified slag with different Fe_2O_3 contents are depicted in Fig. 2a. The analysis reveals that the primary mineral phases present in the slag include α-C_2S, β-C_2S, C_3MS_2, spinel, CF, and RO phases. Previous studies[35] have indicated that Fe_3O_4 and $MgFe_2O_4$ have similar crystal structures, which result in very close diffraction peak angles on their corresponding (220), (311), (400), (511), and (440) crystal planes. It becomes difficult to distinguish between them based on the XRD results. Therefore, in this study, the term "spinel" is used to refer to both Fe_3O_4 and $MgFe_2O_4$. It is interesting to note that the actual results of the modified slag differ from the thermodynamic calculations, as no γ-C_2S was observed. This is because the P element in steel slag can dissolve into dicalcium silicate (β-Ca_2SiO_4) grains. Its presence inhibits the crystallographic transformation of β-Ca_2SiO_4 to γ-Ca_2SiO_4.[36] This suggests that the cooling rate during the actual modification process was relatively fast, preventing the formation of γ-C_2S in the lower temperature range. Furthermore, it is worth noting that β-C_2S is a metastable substance, and its absence in the thermodynamic calculation results can be attributed to the lack of inclusion in the Factsage database. As depicted in Fig. 2a, it is evident that the diffraction peak intensity of spinel of the FC30 modified slag was higher compared to that of the silicate minerals. This observation suggests that a higher Fe_2O_3 content leads to a reduction in the generation of silicate minerals in the modified slag. As the Fe_2O_3 content decreased in the modified slag, there is an observed trend in the diffraction peak intensity of the different mineral phases. Specifically, the diffraction peak intensity of Ca_2SiO_4 gradually increased, while that of the spinel minerals and CF gradually decreased. This indicates that the decrease in Fe_2O_3 content promotes the formation of Ca_2SiO_4. According to the research conducted by Jiang et al.,[37] the combination of CaO and SiO_2 in steel slag to form Ca_2SiO_4 exhibits a strong thermodynamic tendency. A decrease in the Fe_2O_3 content in the slag implies an increase in the relative content of CaO and SiO_2. Therefore, as the Fe_2O_3 content decreases, the content of Ca_2SiO_4 increases significantly.

Figure 2b–e shows the microstructure of SEM-BSD images depicting modified slag samples with varying Fe_2O_3 contents, and the corresponding energy spectrum data are shown in Table S2. In the case of the FC30 modified slag, the C_2S grains exhibited a round and elliptical shape, with a grain size ranging from approximately 20–45 μm. The matrix phase surrounding the C_2S grains consisted of dispersed spinel phase and CF. In the FC25 modified slag, a spindle-shaped phase of C_3MS_2 was observed at the grain boundary of C_2S. The grain size of C_2S in the FC25 modified slag ranged from approximately 5.5–30 μm. Furthermore, compared to the FC30 modified slag, the grain size of C_2S in the FC25 modified slag increased to about 25–50 μm. The grain morphology of C_2S in the FC25 modified slag exhibited not only round and oval shapes but also plate-like structures. In the modified slag with decreased content of spinel phase and CF as the matrix phase, the RO phase exhibited an irregular elliptical shape. Additionally, the grain size of C_3MS_2 increased to approximately 7–50 μm. In the FC20 modified slag, the content of C_2S was further increased, resulting in a reduction in grain size. Additionally, the content of the matrix phase was further reduced in comparison to previous modifications. In the FC15 modified slag, the content of C_2S continued to increase. The grains of C_2S predominantly exhibited a plate-like morphology, while the matrix phase nearly disappeared in this composition. Instead, the C_3MS_2 and RO phases were distributed within the gaps between the C_2S grains. The microstructure observed in the SEM-BSD images aligns with the results obtained from thermodynamic calculations and the XRD analysis. Specifically, the decrease in Fe_2O_3 content in the modified slag resulted in an increase in the content of C_2S while reducing the content of spinel and CF

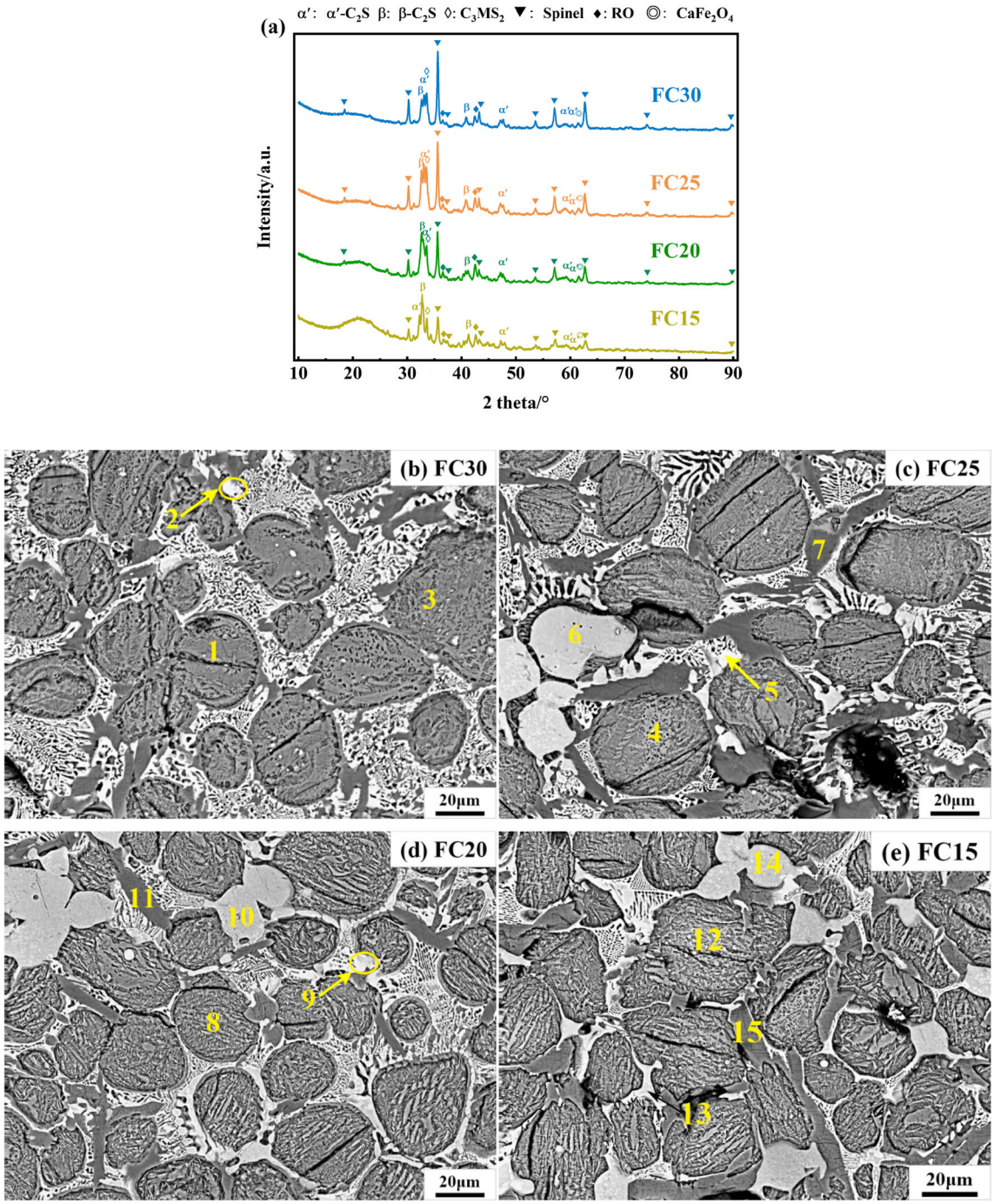

Fig. 2. XRD pattern and SEM microstructures of modified slag with different Fe_2O_3 contents: (a) XRD pattern of modified slag with different Fe_2O_3 contents; (b) SEM microstructure of FC30 modified slag; (c) SEM microstructure of FC25 modified slag; (d) SEM microstructure of FC20 modified slag; (e) SEM microstructure of FC15 modified slag. The figures in the graph are energy spectrum data numbers, and the energy spectrum data are shown in Table S2.

phases. Consequently, reducing the Fe_2O_3 content was found to promote the leaching of Ca elements.

Influence of Fe_2O_3 Content on CLR of Steel Slag

Figure 3 illustrates the CLR and leaching residue XRD patterns of modified slag samples with varying Fe_2O_3 contents. Figure 3a shows that, as the Fe_2O_3 content in the modified slag decreased, the CLR gradually increased. When the Fe_2O_3 content decreased from 30 wt.% to 15 wt.%, the CLR increased from 92.01% to 98.26%. This trend in the CLR aligns with the findings obtained from the XRD and SEM analyses. Indeed, as the Fe_2O_3 content in the modified slag decreased, the content of C_2S increased while the content of spinel phase

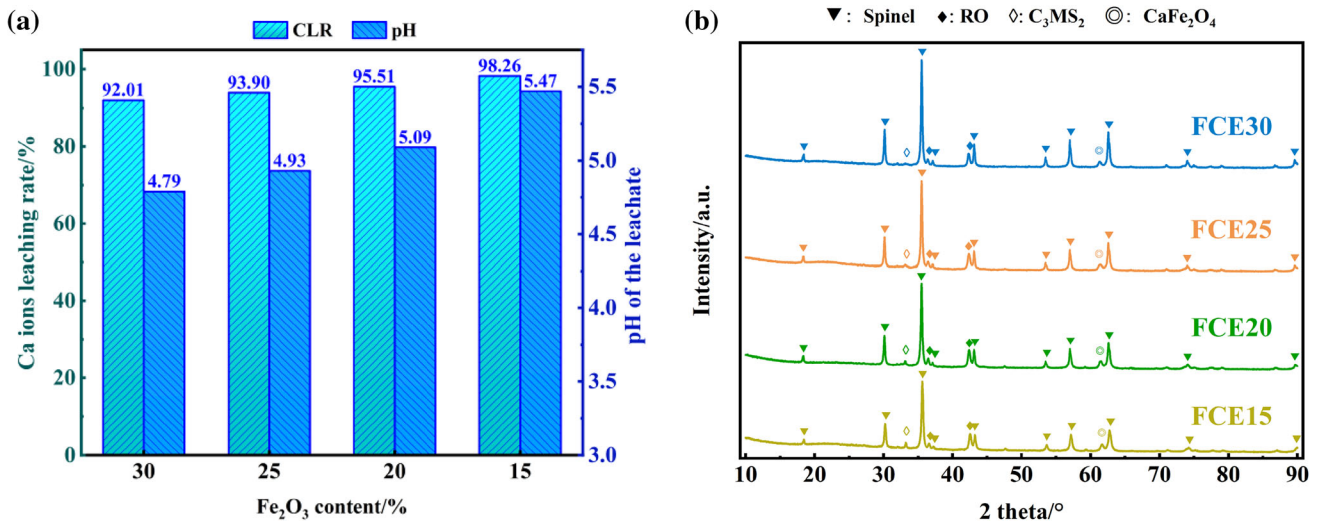

Fig. 3. CLR and leaching residue XRD pattern of modified slag with different Fe_2O_3 contents: (a) CLR of modified slag with different Fe_2O_3 contents; (b) leaching residue XRD pattern of modified slag with different Fe_2O_3 contents.

and CF decreased. Consequently, a larger proportion of Ca elements in the slag was present in the silicate minerals, in particular C_2S. As a result, the CLR gradually increased. The pH of the leachate of the modified slag correlates with the content of Fe_2O_3, following the trend observed in the CLR. As the Fe_2O_3 content decreased, the pH of the leachate gradually increased. When the Fe_2O_3 content was reduced to 15 wt.%, the pH of the leachate reached its highest value of 5.47.

Figure 3b displays the XRD pattern of the leaching residue of modified slag samples with different Fe_2O_3 contents. After the leaching reaction, the diffraction peaks corresponding to α-C_2S, β-C_2S, and C_3MS_2 in the original modified slag were essentially absent. The main mineral composition of the leaching residue consists of the spinel phase and the RO phase. Additionally, there are weak diffraction peaks observed for C_3MS_2 and CF in the residue. Similar to the modified slag, the diffraction peak intensity of the spinel phase in the leaching residue gradually decreased with the decrease in Fe_2O_3 content. This suggests that the spinel phase does not actively participate in the leaching reaction and remains relatively stable during the leaching process. Indeed, the observation that the remaining minerals in the leaching residue of modified slag with different Fe_2O_3 contents, when the basicity was 2, were all iron-bearing minerals, indicating that acetic acid can selectively react with the minerals in the modified slag. After the leaching reaction, the silicate minerals in the modified slag have essentially disappeared, while the iron-bearing minerals were retained. This implies that, under the specific experimental conditions, the modified slag can effectively release Ca elements while enabling the efficient recovery of Fe elements. This outcome is of great significance for achieving the maximum recovery of valuable metal elements present in steel slag.

Influence of MgO Content on Mineral Composition and CLR of Steel Slag

Thermodynamic Analysis

The thermodynamic calculation results of modified slag with different MgO contents are presented in Fig. 4. As the temperature decreased, the liquid phase content in the slag gradually decreased, while the precipitation of α-C_2S and β-C_2S occurred successively. As the temperature decreased, α-C_2S and β-C_2S phases disappeared, and, instead, C_3MS_2, C_2F, CF, and melilite phases gradually precipitated. At temperatures below 350°C, the content of C_3MS_2 gradually decreased, while the content of γ-C_2S rapidly increased. When the modified slag was cooled to room temperature, the resulting mineral phases in the slag typically included γ-C_2S, spinel, C_2F, CF, etc. With the increase of MgO content in the modified slag, the observed trends in Fig. 4 show that the content of γ-C_2S gradually decreased. Additionally, the crystallization temperature range of C_3MS_2 gradually increased, and the precipitation amount of C_3MS_2 also increased. That is, the addition of MgO promotes the formation of C_3MS_2 in the modified slag, leading to a relatively reduced content of C_2S. At the same time, the narrow temperature range of α-C_2S and β-C_2S was related to the gradual increase in the initial temperature of C_3MS_2. The amount of spinel phase precipitation increased with the increase of MgO content in the modified slag. This indicates that a higher concentration of MgO promotes the combination of MgO with Fe_2O_3, resulting in the formation of more $MgFe_2O_4$ spinel.

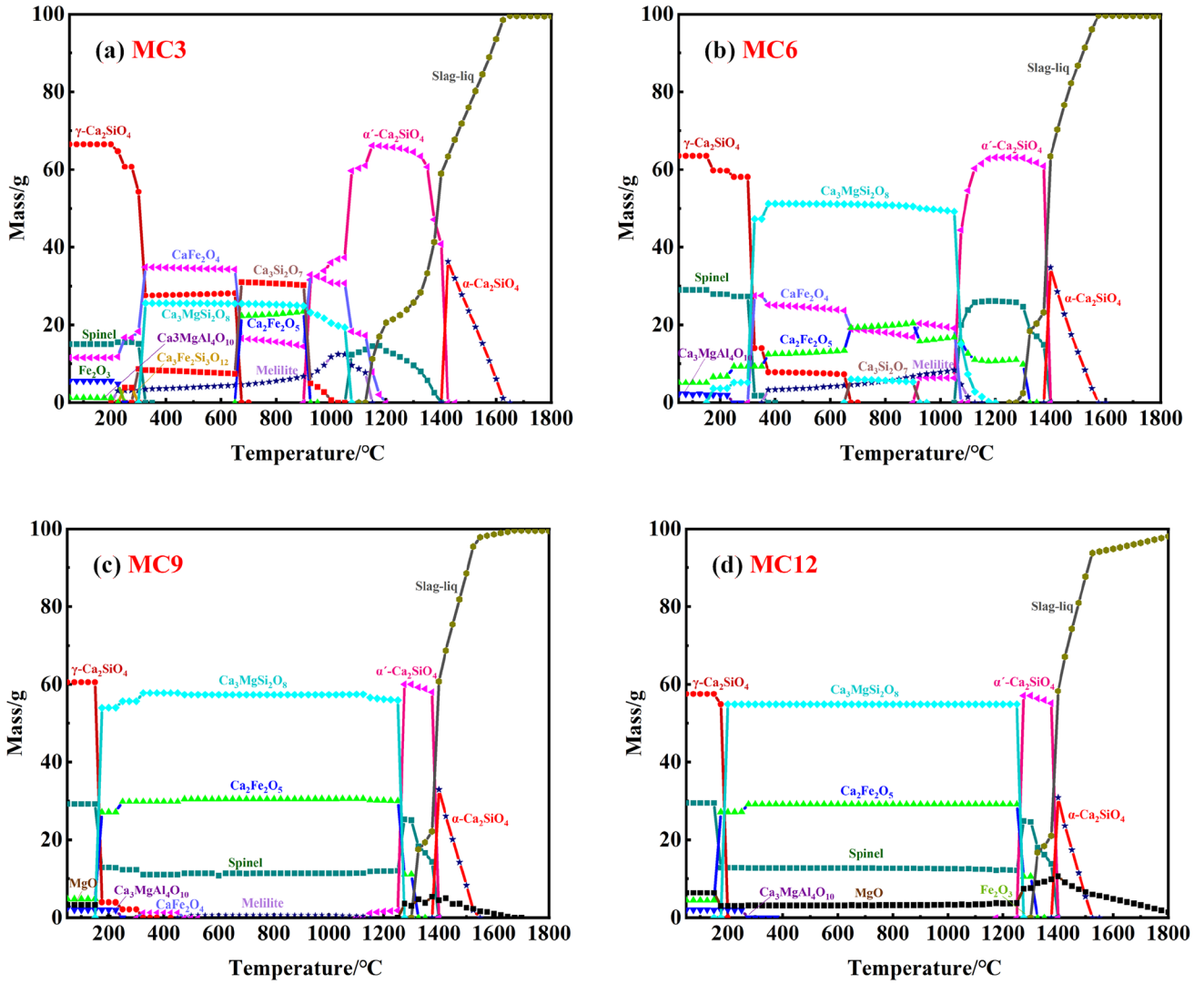

Fig. 4. Thermodynamic calculation results of modified slag with different MgO contents: (a) thermodynamic calculation results of MC3 modified slag; (b) thermodynamic calculation results of MC6 modified slag; (c) thermodynamic calculation results of MC9 modified slag; (d) thermodynamic calculation results of MC12 modified slag.

Influence of MgO Content on Mineral Composition of Steel Slag

The XRD pattern depicted in Fig. 5a shows the mineral components of the modified slag with varying MgO contents. The major mineral phases detected in the MgO modified slag include α-C_2S, β-C_2S, C_3MS_2, spinel, CF, and RO phases. The diffraction peaks corresponding to α-C_2S and β-C_2S in the slag show a gradual decrease with the increase of MgO content, aligning with the thermodynamic calculation results. This observation confirms that the increased MgO content is not favorable for the formation of C_2S. Furthermore, the diffraction peak intensity of the RO phase in the modified slag shows a gradual increase, indicating that the increase in MgO content results in a higher formation of solid solution between MgO and FeO, leading to the RO phase. This can be attributed to the relatively close ionic radii of Mg^{2+} (0.083 nm) and Fe^{2+} (0.078 nm). Due to their similar sizes, MgO can dissolve with FeO in any proportion. Additionally, the shift of the diffraction peak of the RO phase to a higher angle can be observed. This shift is attributed to the reduction in the lattice constant of the RO phase due to the increased incorporation of MgO solid solution. As more MgO was incorporated into the FeO lattice, the lattice constant of the RO phase became smaller, resulting in the observed shift of the diffraction peak to higher angles.

The SEM microstructure of the modified slag with various MgO contents is presented in Fig. 5b–e, and the corresponding energy spectrum data are provided in Table S3. The microstructural analysis reveals the presence of several mineral phases in the MgO modified slag, including C_2S, C_3MS_2, spinel, and the RO phase. In the MC3 modified slag, the C_2S grains exhibit a plate-like morphology with a grain size ranging from 25 μm to 60 μm. The

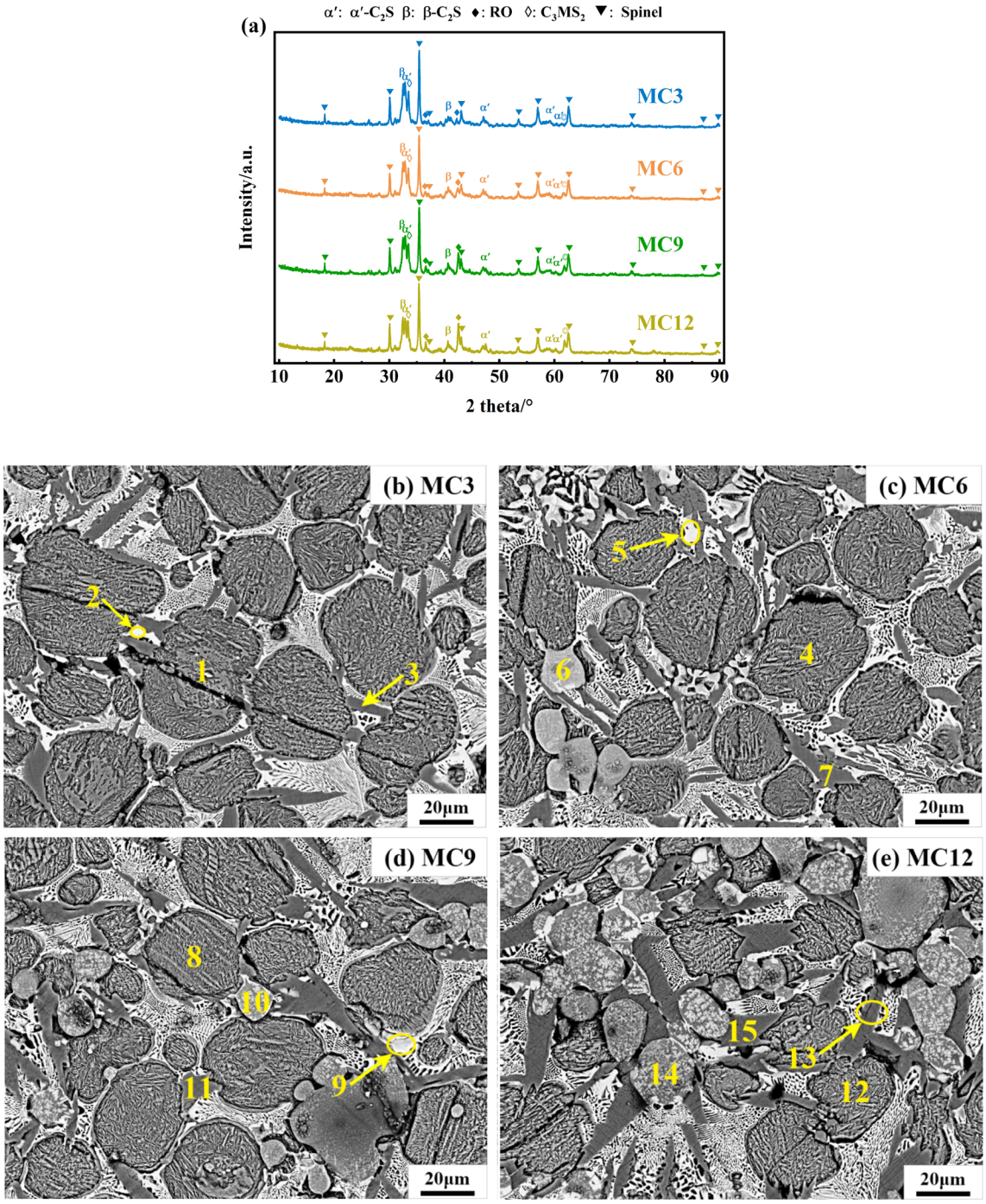

Fig. 5. XRD pattern and SEM microstructure of modified slag with different MgO contents: (a) XRD pattern of modified slag with different MgO contents; (b) SEM microstructure of MC3 modified slag; (c) SEM microstructure of MC6 modified slag; (d) SEM microstructure of MC9 modified slag; (e) SEM microstructure of MC12 modified slag. The figures in the graph are energy spectrum data numbers, and the energy spectrum data are shown in Table S3.

spinel phase and CF were distributed around the C_2S grains, serving as the matrix phases. Additionally, the C_3MS_2 phase was present at the boundary of the C_2S grains, appearing in a spindle shape with a grain size of 7–35 μm. In the MC6 modified slag, the grain size of C_2S decreased to approximately 20–42 μm compared to the MC3 modified slag. Additionally, in the MC6 modified slag, an elliptical light gray RO phase emerged. In the MC9 and MC12 modified slag, the content of C_2S was further reduced compared to previous modifications. Simultaneously, the content of the RO phase was further increased. Notably, in the MC9 and MC12 modified slag, the RO phase starts to appear as dark gray spots. This change in color was attributed to the increased amount of MgO dissolved in the RO

phase. By examining Table S3 and considering the atomic ratios, it became apparent that the atomic ratio of Mg atoms in the RO phase gradually increased with the increment of MgO content in the modified slag. This ratio rises from 7.23% in the MC3 modified slag to 30.94% in the MC12 modified slag. Previous studies[38] have indicated that the RO phase can be divided into two types based on the K_m value (K_m = MgOwt.%/(FeOwt.% + MnOwt.%)). When $K_m > 1$, it corresponds to ferrite solid solution, while $K_m < 1$ corresponds to brucite solid solution. Therefore, it can be observed that the RO phase in question is brucite solid solution since the value of K_m is greater than 1.

Influence of MgO Content on CLR of Steel Slag

Figure 6 presents the CLR and leaching residue XRD pattern of the modified slag with varying MgO contents. It is evident that, as the MgO content in the modified slag increased from 3 wt.% to 12 wt.%, the CLR decreased from 97.38% to 92.62%. This finding suggests that an elevated MgO content may have a detrimental effect on the leaching efficiency of Ca ions of the modified slag. Indeed, despite the decrease in the CLR with the increase of MgO content in the modified slag, it is worth noting that the CLR for all four groups of modified slag remained above 90%. This suggests that the variation in MgO content had a limited influence on the overall CLR. Indeed, based on the information provided earlier, the increase in MgO content primarily led to an increase in the content of the RO phase in the modified slag. The RO phase does not combine with the Ca element to form minerals with low reactivity. As a result, the presence of the RO phase, which is rich in MgO, has little influence on the CLR. With an increase in MgO content, the pH of the leachate initially decreased and then increased. This phenomenon can be attributed to the following explanation: When the MgO content was below 6 wt.%, higher MgO content results in a reduction in the C_2S content present in the modified slag. Subsequently, the amount of acetic acid consumed during the leaching process decreased. As a consequence, there is a decrease in the release of H^+ ions in the leachate, leading to a lower pH. When the MgO content exceeds 6 wt.%, a portion of the MgO exists in excess and remains in a free state within the modified slag. This excess MgO can contribute to basicity in the leaching system. During the leaching process, the alkaline f-MgO (free MgO) can participate in leaching reactions, influencing the pH of the leachate. As a result, the pH of the leachate increased.

As can be seen from Fig. 6b, the main minerals identified in the leaching residue were iron-bearing, specifically the spinel phase and the RO phase. Furthermore, weak diffraction peaks of C_3MS_2 and CF were observed in the XRD pattern of the leaching residue. These diffraction peaks indicate the presence of these minerals in the modified slag. The intensities of the diffraction peaks corresponding to C_3MS_2 and CF in the leaching residue were found to increase with the increase in MgO content within the modified slag. This observation is consistent with the results of the CLR. The elevated presence of unreacted C_3MS_2 and CF in the modified slag leads to a decrease in the CLR. In the case of the modified slag with varying MgO content, the mineral composition of the leaching residue indicates that the silicate minerals have been consumed during the leaching reaction. As a result, the remaining minerals in the slag predominantly consist of iron-bearing minerals. Indeed, when the basicity of the modified slag was 2, the variation in MgO content does not significantly impact the mineral composition of the slag. In this case, the leaching residue primarily consists of iron minerals, indicating that effective recovery of both Ca and Fe

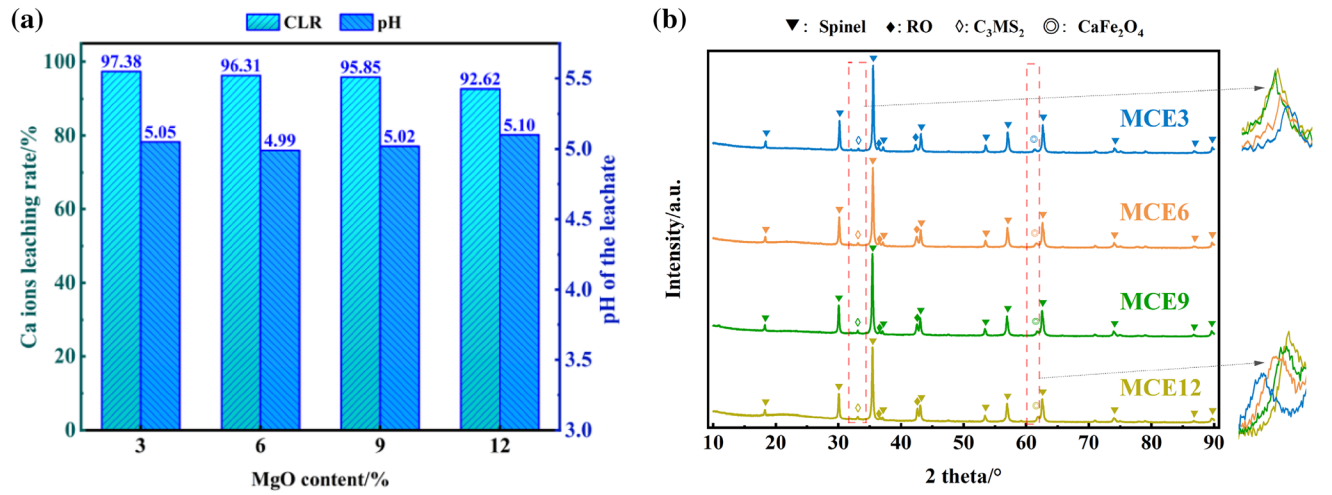

Fig. 6. CLR and leaching residue XRD pattern of modified slag with different MgO contents: (a) CLR of modified slag with different MgO contents; (b) leaching residue XRD pattern of modified slag with different MgO contents.

elements from the slag can be achieved under the experimental conditions.

Influence of Al_2O_3 Content on Mineral Composition and CLR of Steel Slag

Thermodynamic Analysis

According to the thermodynamic calculation results shown in Fig. 7, for the AC3 and AC6 modified slag with different Al_2O_3 contents, during this cooling process, α-C_2S and α′-C_2S precipitate successively. The content of α-C_2S in the modified slag experienced a rapid decrease at 1200°C and completely disappeared at 900°C. Simultaneously, the precipitation of C_3MS_2 began at 1100°C. C_3MS_2 then remained stable in the temperature range of 350–1050°C. The precipitation of γ-C_2S in the modified slag began at 700°C and reached its maximum level at 200°C. During the cooling process, the iron-bearing minerals, including the spinel phase, C_2F, and CF, precipitate successively. When the modified slag was cooled to room temperature, several stable minerals were observed in the slag. These minerals included γ-C_2S, the spinel phase, CF, $CaMg_2Al_{16}O_{27}$, and Fe_2O_3. Additionally, during the cooling process of these two groups of modified slag, there was also the precipitation of melilite. Furthermore, as the Al_2O_3 content in the modified slag increased, the precipitation of melilite gradually increased. For the AC9 modified slag, there was no precipitation of α-C_2S during the cooling process; instead, melilite and α-C_2S precipitated together. For the AC12 slag, the precipitation of melilite happened earlier than that of α-C_2S. Furthermore, the amount of melilite precipitated was significantly increased compared to the first three groups of modified slag. Based on Fig. 7, it is evident that, as the Al_2O_3 content in the modified

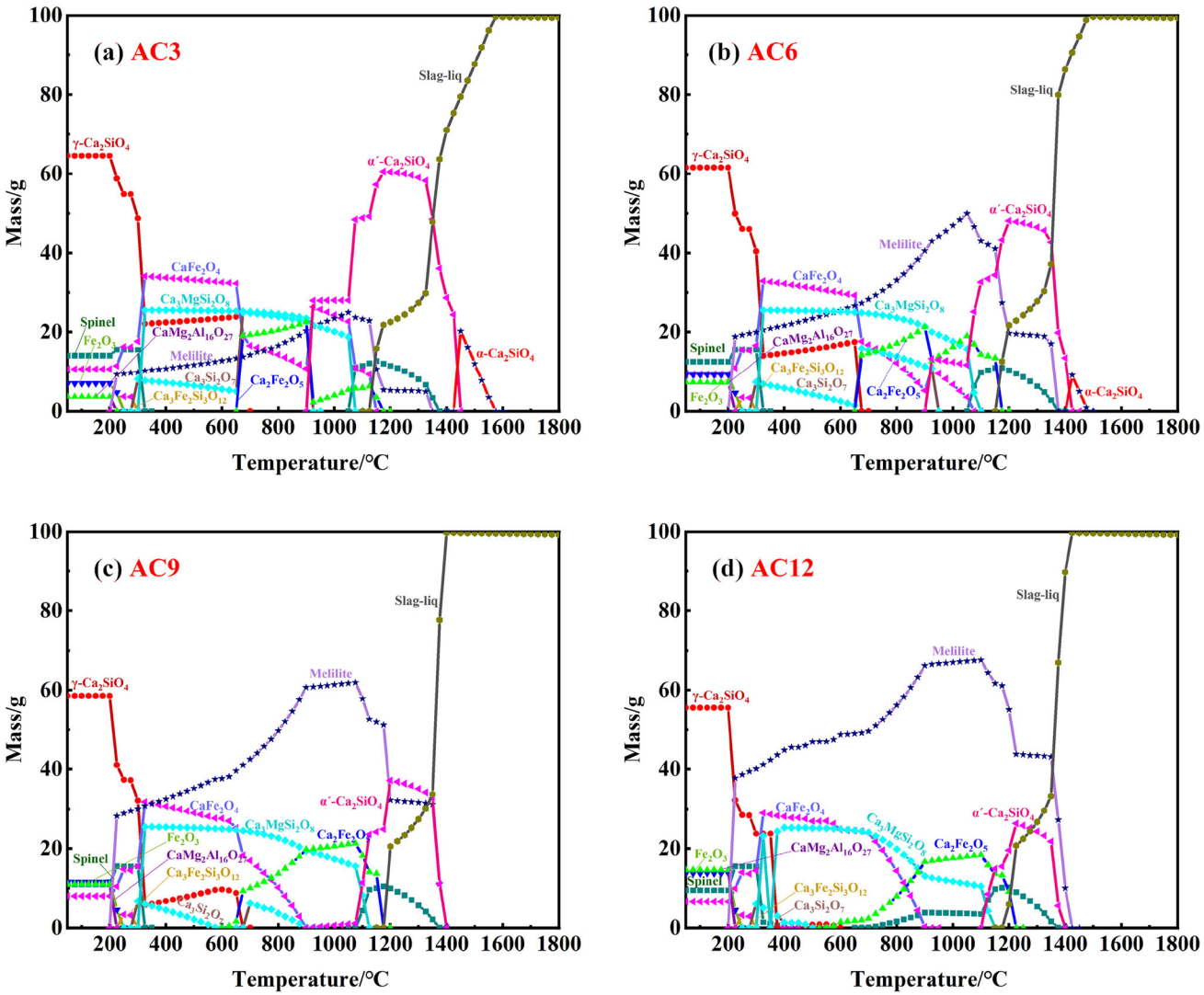

Fig. 7. Thermodynamic calculation results of modified slag with different Al_2O_3 contents: (a) thermodynamic calculation results of AC3 modified slag; (b) thermodynamic calculation results of AC6 modified slag; (c) thermodynamic calculation results of AC9 modified slag; (d) thermodynamic calculation results of AC12 modified slag.

slag increased, the precipitation amount of γ-C_2S progressively decreased, while the precipitation amount of melilite gradually increased. This indicates that the presence of Al_2O_3 hinders the formation of γ-C_2S and enhances the formation of melilite.

Influence of Al_2O_3 Content on Mineral Composition of Steel Slag

Figure 8a shows the XRD pattern of modified slag samples with varying Al_2O_3 contents. In the case of the AC3 and AC6 modified slags, the dominant mineral compositions observed were α-C_2S, β-C_2S, C_3MS_2, $MgFeAlO_4$, and RO phases. In the AC9 modified slag, the diffraction peaks corresponding to α-C_2S and C_3MS_2 were no longer present. Instead, the appearance of $Ca_3Al_{0.84}Fe_{1.16}Si_3O_{12}$ was observed. Furthermore, in the AC12 modified slag, $Ca_3Al_2Si_3O_{12}$ (C_3AS_3) emerges as a distinct diffraction peak. A progressive decrease in the diffraction peak intensity of β-C_2S was observed in the modified slag samples from AC3 to AC12. This trend indicates that an increase in Al_2O_3 content in the modified slag hampered the formation of silicate minerals while promoting the formation of aluminosilicate minerals. In contrast to the presence of the $MgFe_2O_4$ spinel phase observed in the previous studies, the Al_2O_3 modified slag exhibited the appearance of the $MgFeAlO_4$ spinel phase. This discrepancy can be attributed to the difference in Al_2O_3 content between the two sets of studies. The earlier studies involved low Al_2O_3 content in the modified slag (≤ 1 wt.%), whereas the current study in this section utilized modified slag with Al_2O_3 content ranging from 3 wt.% to 12 wt.%. The increase in Al_2O_3 content leads to the dissolution of some Al atoms into the lattice of the $MgFe_2O_4$ spinel phase, resulting in the formation of the $MgFeAlO_4$ spinel phase. As depicted in Fig. 8a, it can be seen that, with the rise in Al_2O_3 content, the diffraction peak corresponding to the $MgFeAlO_4$ spinel phase gradually shifted towards higher angles. This can be attributed to the decrease in the lattice constant of the spinel phase caused by an increased solid solution of Al atoms. The high-angle shift of the diffraction peak of the $MgFeAlO_4$ spinel phase was a direct consequence of this change in lattice constant.

Figure 8b–e presents the SEM microstructure of the modified slag samples with varying Al_2O_3 contents, while Table S4 provides the corresponding energy spectrum data. In the case of the AC3 modified slag, the main mineral phases observed were C_2S, C_3MS_2, and $MgFeAlO_4$. In the AC3 modified slag, C_2S was present in elliptic and plate-like morphologies, with a grain size ranging from approximately 14–50 μm. $MgFeAlO_4$ exists as a matrix phase, while C_3MS_2 is observed in a spindle shape along the boundaries of C_2S grains. In the AC6 modified slag, the content of C_2S decreased compared to AC3, and its grain size reduced to approximately 12–42 μm. C_3MS_2 appeared in a needle-like form. In the AC9 modified slag, there was no distinct C_2S grain observed. From the locally magnified SEM images, it can be observed that dark spindle-shaped substances are present in the slag. According to the energy spectrum data from Table S4, the main components of this substance are Ca and Si, with a Ca/Si ratio close to 2:1. This suggests that the substance is partially crystallized Ca_2SiO_4 that has not completed its crystalline growth. In addition, $Ca_3Al_{0.84}Fe_{1.16}Si_3O_{12}$ exists in an amorphous form surrounding Ca_2SiO_4, while $MgFeAlO_4$ exists as the matrix phase. In the case of the AC12 modified slag, compared to the AC9 modified slag, the spindle-shaped Ca_2SiO_4 grain size is smaller, and $Ca_3Al_2Si_3O_{12}$ and $MgFeAlO_4$ as matrix phases are dispersed around Ca_2SiO_4. The AC9 and AC12 modified slags exhibit different microstructural features compared to other modified slags. There are no clearly defined circular or elliptical Ca_2SiO_4 grains. This is attributed to the higher viscosity of the Al_2O_3 modified slag. As shown in Fig. S2, the viscosity of Al_2O_3 is significantly higher than that of the Fe_2O_3 modified slag and the MgO modified slag. Additionally, the modified slags with 9% and 12% Al_2O_3 content have even higher viscosities. During the process of cooling from the molten state to room temperature, the Ca and Si atoms in the modified slag undergo diffusion and locally enrich. After enrichment, they undergo nucleation and crystalline growth to form Ca_2SiO_4 grains.[39] When the viscosity of the molten slag is too high, the diffusion of Ca and Si components becomes difficult, which hinders the growth of Ca_2SiO_4. This leads to the distinct morphology of Ca_2SiO_4 grains in the AC9 and AC12 modified slags compared to other modified slags.

Influence of Al_2O_3 Content on CLR of Steel Slag

Figure 9 shows the CLR and leaching residue XRD pattern of the modified slag with varying Al_2O_3 contents. It can be observed from Fig. 9a that, as the Al_2O_3 content increased from 3 wt.% to 12 wt.%, the CLR decreased from 92.85% to 88.68%. In comparison to the MgO modified slag, the CLR of the Al_2O_3 modified slag was lower. This can be attributed to the fact that the increase in Al_2O_3 content not only affected the formation of the non-calcium-containing mineral spinel phase but also impacted the formation of the calcium-containing mineral, C_3AS_3. Indeed, calcium-aluminosilicate minerals have generally shown lower reactivity compared to other minerals. As a result, an increase in Al_2O_3 content will have a significant impact on the CLR of modified slag. The pH of the leachate of the modified slag exhibits a decrease with increasing Al_2O_3 content. The pH values decreased from 4.90 to 4.58 as the Al_2O_3 content increased. This indicates that the increase in Al_2O_3 content has a

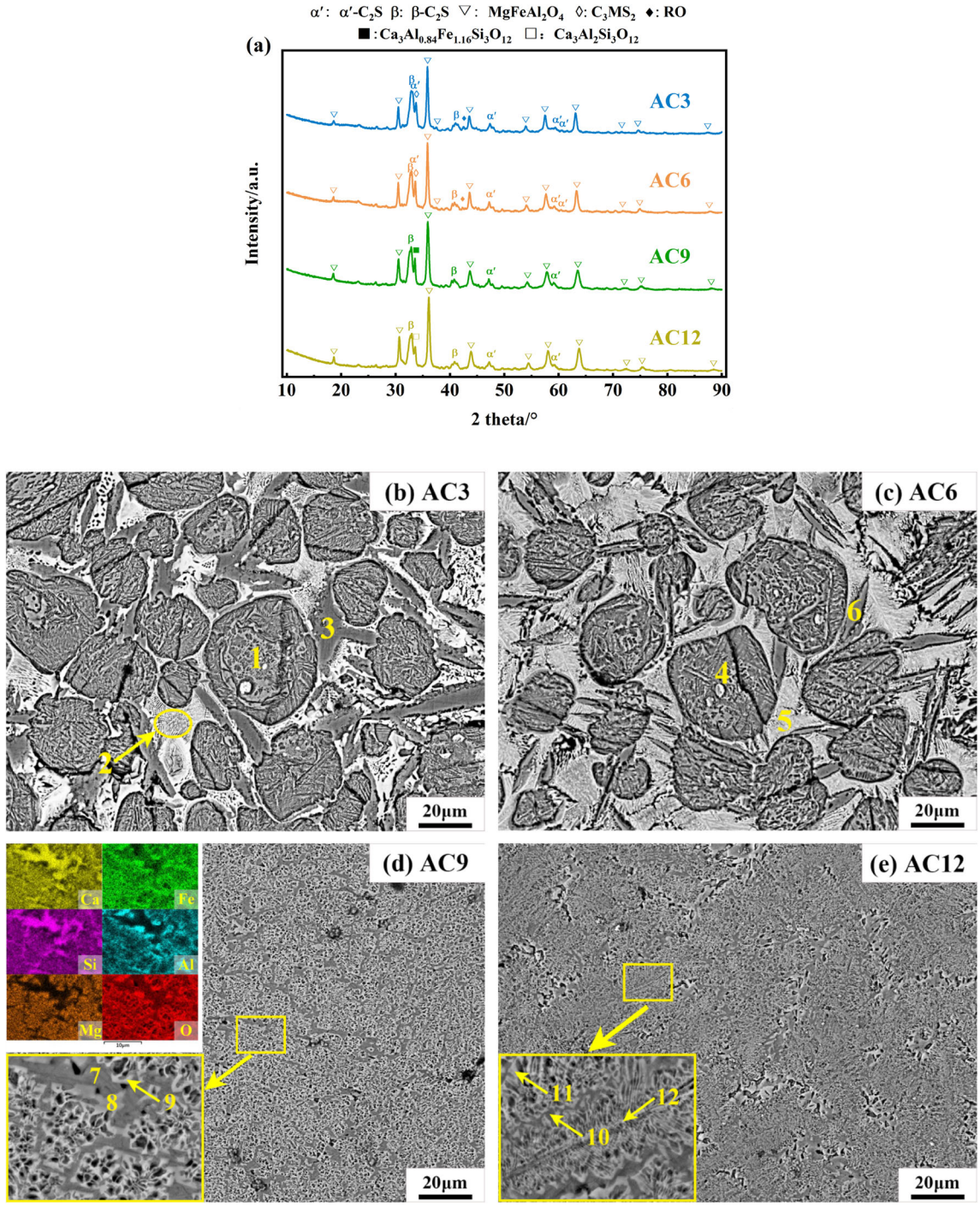

Fig. 8. XRD pattern and SEM microstructure of modified slag with different Al_2O_3 contents: (a) XRD pattern of modified slag with different Al_2O_3 contents; (b) SEM microstructure of AC3 modified slag; (c) SEM microstructure of AC6 modified slag; (d) SEM microstructure of AC9 modified slag; (e) SEM microstructure of AC12 modified slag. The figures in the graph are energy spectrum data numbers, and the energy spectrum data are shown in Table S4.

significant impact on the pH of the leachate, resulting in a lower pH value.

It can be observed from Fig. 9b that the main minerals of the leaching residue include the $MgFeAlO_4$ spinel phase and the RO phase. Additionally, there were small amounts of C_3MS_2, $Ca_3Al_{0.84}Fe_{1.16}Si_3O_{12}$, and C_3AS_3 present in the residue. These results indicate that, when the basicity was 2, the variation in Al_2O_3 content does not significantly affect the mineral composition of the modified slag. The leaching residue was rich in iron minerals. Therefore, under these experimental

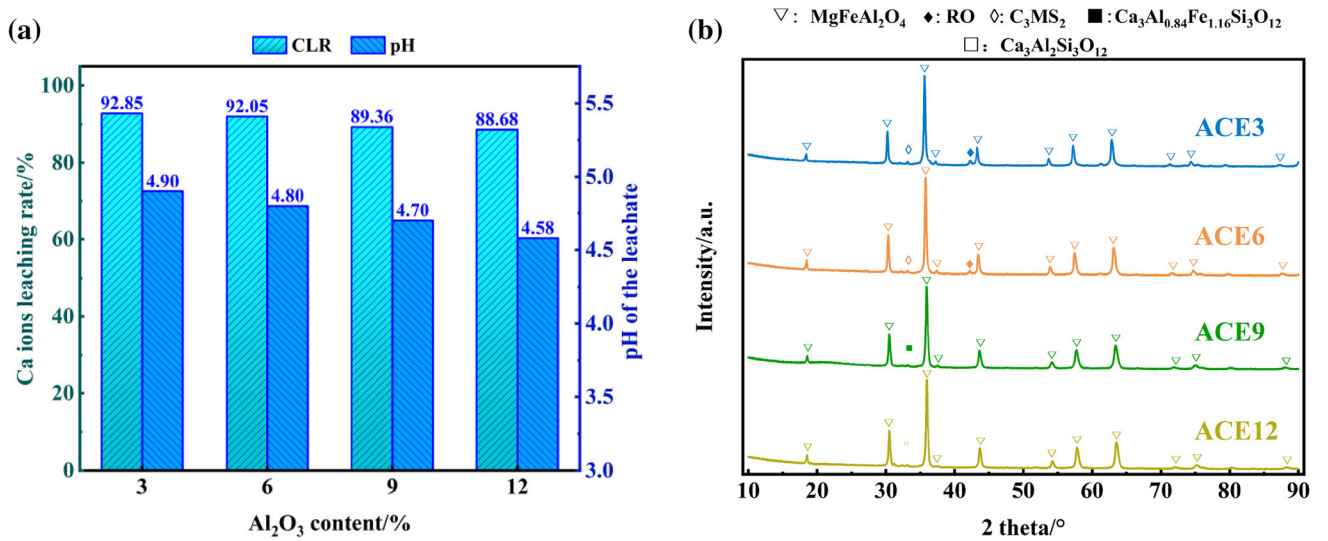

Fig. 9. CLR and leaching residue XRD pattern of modified slag with different Al_2O_3 contents: (a) CLR of modified slag with different Al_2O_3 contents; (b) leaching residue XRD pattern of modified slag with different Al_2O_3 contents.

conditions, effective recovery of Ca and Fe elements from the slag can still be achieved.

CONCLUSION

The effects of Fe_2O_3, MgO, and Al_2O_3 contents on the mineral composition and the CLR of steel slag were investigated. The main conclusions can be summarized as follows:

(1) As the Fe_2O_3 content in the modified slag decreased, the content of C_2S in the slag increased. Consequently, the CLR gradually increased. Specifically, when the Fe_2O_3 content of the modified slag decreased from 30 wt.% to 15 wt.%, the CLR increased from 92.01% to 98.26%.

(2) As the MgO content increased, the content of C_2S in the slag decreased. However, MgO does not react significantly with the Ca element to form minerals with low reactivity. As a result, its influence on the CLR was limited. Specifically, when the MgO content in the modified slag increased from 3 wt.% to 12 wt.%, the CLR decreased from 97.38% to 92.62%.

(3) The CLR of Al_2O_3 modified slag was found to be low. This is because calcium-aluminosilicate minerals generally exhibit poor reactivity, so the increase in Al_2O_3 content has a significant impact on the CLR of the modified slag. Specifically, when the Al_2O_3 content in the modified slag increased from 3 wt.% to 12 wt.%, the CLR decreased from 92.85% to 88.68%.

(4) At a basicity of 2, the modified slag can effectively release Ca elements while also enabling the efficient recovery of Fe elements. Such findings are of utmost importance for maximizing the recovery of valuable metal elements from steel slag.

SUPPLEMENTARY INFORMATION

The online version contains supplementary material available at https://doi.org/10.1007/s11837-023-06342-z.

ACKNOWLEDGEMENTS

The authors would like to acknowledge University of Science and Technology Beijing and Shougang Research Institute of Technology for providing the support.

CONFLICT OF INTEREST

On behalf of all authors, the corresponding author states that there is no conflict of interest.

REFERENCES

1. H.N. Zhang, Q.Q. Zuo, C. Wei, X. Lin, J.P. Dong, C.F. Liao, and A.J. Xu, *Sci. Total. Environ.* 738, 139747 https://doi.org/10.1016/j.scitotenv.2020.139747 (2020).
2. N. Council, *Climate Change: Evidence, Impacts, and Choices: Set of 3 Booklets* (National Academies Press, Los Angeles, 2012), pp20–29.
3. CO_2. Earth. "Trends in Atmospheric Carbon Dioxide" (CO_2. Earth. 2007), https://www.CO2.earth/. Accessed 2 Sept 2021. Accessed 2 Aug 2023.
4. S.O. Omale, T.S.Y. Choong, L.C. Abdullah, S.I. Siajam, and M.W. Yip, *Heliyon* 5, e02602 https://doi.org/10.1016/j.heliyon.2019.e02602 (2019).
5. H.N. Zhang, J.H. Dong, H. Li, H.H. Xiong, and A.J. Xu, *JOM* 70, 938 https://doi.org/10.1007/s11837-017-2591-4 (2018).

6. J.Q. Gao, C. Li, W.Z. Liu, J.P. Hu, L. Wang, Q. Liu, B. Liang, H.R. Yue, G.Q. Zhang, D.M. Luo, and S.Y. Tang, *Chin. J. Chem. Eng.* 27, 157 https://doi.org/10.1016/j.cjche.2018.04.012 (2019).
7. Q. Liu, W.Z. Liu, J.P. Hu, L. Wang, J.Q. Gao, B. Liang, H.R. Yue, G.Q. Zhang, D.M. Luo, and C. Li, *J. Clean. Prod.* 197, 242 https://doi.org/10.1016/j.jclepro.2018.06.150 (2018).
8. J.P. Hu, W.Z. Liu, L. Wang, Q. Liu, F. Chen, H.R. Yue, B. Liang, L. Lu, Y. Wang, G.Q. Zhang, and C. Li, *J. Energy Chem.* 26, 927 https://doi.org/10.1016/j.jechem.2017.06.009 (2017).
9. M. Dri, A. Sanna, and M.M. Maroto-Valer, *Appl. Energy* 113, 515 https://doi.org/10.1016/j.apenergy.2013.07.064 (2014).
10. S. Kodama, T. Nishimoto, N. Yamamoto, K. Yogo, and K. Yamada, *Energy* 33, 776 https://doi.org/10.1016/j.energy.2008.01.005 (2008).
11. M. Owais, M. Jarvinen, P. Taskinen, and A. Said, *J. CO2 Util.* 31, 1 https://doi.org/10.1016/j.jcou.2019.02.014 (2019).
12. R. Ragipani, S. Bhattacharya, and A.K. Suresh, *Proc. Math. Phys. Eng. Sci.* 475, 20180830 https://doi.org/10.1098/rspa.2018.0830 (2019).
13. Y.B. Luo, D.F. He, and H.B. Zhao, *JOM* 75, 1019 https://doi.org/10.1007/s11837-022-05556-x (2022).
14. Y.B. Luo and D.F. He, *Environ. Sci. Pollut. Res.* 28, 49383 https://doi.org/10.1007/s11356-021-15254-x (2021).
15. P. Nielsen, M.A. Boone, L. Horckmans, and R. Snellings, *M. Quaghebeur.* 36, 124 https://doi.org/10.1016/j.jcou.2019.10.022 (2019).
16. J. Kim, B.K. Sovacool, M. Bazilian, S. Griffiths, J. Lee, M. Yang, and J.J.E.R. Lee, *Science* 89, 102565 https://doi.org/10.1016/j.erss.2022.102565 (2022).
17. S.H. Kim, S. Jeong, H. Chung, and K. Nam, *Waste Manag.* 103, 122 https://doi.org/10.1016/j.wasman.2019.12.019 (2020).
18. J.Y. Wang, M. Zhong, P.F. Wu, S.K. Wen, L. Huang, and P. Ning, *Chem. Bio. Eng. Rev.* 8, 1 https://doi.org/10.1002/cben.202000021 (2021).
19. Y.B. Luo and D.F. He, *JOM* 74, 1958 https://doi.org/10.1007/s11837-022-05217-z (2022).
20. Y. Luo and D. He, *J. Sust. Metall.* 7, 947 https://doi.org/10.1007/s40831-021-00384-w (2021).
21. W.J.J. Huijgen, G.J. Witkamp, and R.N.J. Comans, *Environ. Sci. Technol.* 39, 9676 https://doi.org/10.1021/es050795f (2005).
22. C.Y. Wang, W.J. Bao, Z.C. Guo, and H.Q. Li, *Acta Metall. Sin.-Engl. Lett.* 31, 771 https://doi.org/10.1007/s40195-017-0694-0 (2018).
23. N.L. Ukwattage, P.G. Ranjith, and X. Li, *Measurement* 97, 15 https://doi.org/10.1016/j.measurement.2016.10.057 (2017).
24. M. Bilen, M. Altiner, and M. Yildirim, *Part. Sci. Technol.* 36, 368 https://doi.org/10.1080/02726351.2016.1267285 (2018).
25. Y. Sun, M.S. Yao, J.P. Zhang, and G. Yang, *Chem. Eng. J.* 173, 437 https://doi.org/10.1016/j.cej.2011.08.002 (2011).
26. T.H. Su, H.J. Yang, Y.H. Shau, E. Takazawa, and Y.C. Lee, *J. Environ. Sci. (China)* 41, 99 https://doi.org/10.1016/j.jes.2015.06.012 (2016).
27. D. Wang, J. Chang, and W.S. Ansari, *J. CO2 Util.* 34, 87 https://doi.org/10.1016/j.jcou.2019.06.001 (2019).
28. T.H. Su, H.J. Yang, Y.H. Shau, E. Takazawa, and Y.C. Lee, *J. Environ. Sci.* 41, 99 https://doi.org/10.1016/j.jes.2015.06.012 (2016).
29. S. Lee, J.W. Kim, S. Chae, J.H. Bang, and S.W. Lee, *J. CO2 Util.* 16, 336 https://doi.org/10.1016/j.jcou.2016.09.003 (2016).
30. Q. Zhao, J.Y. Li, K.W. You, and C.J. Liu, *Process Saf. Environ. Protect.* 135, 81 https://doi.org/10.1016/j.psep.2019.12.012 (2020).
31. X. Mei, Q. Zhao, J. Zhou, X. Lang, Y. Min, H. Saxén, and R. Zevenhoven, *J. Sust. Metall.* 7, 391 https://doi.org/10.1007/s40831-021-00374-y (2021).
32. D.F. He, L. Yang, Y.B. Luo, *Chemosphere* (2023, in process).
33. C.W. Bale, E. Bélisle, P. Chartrand, S.A. Decterov, G. Eriksson, K. Hack, I.H. Jung, Y.B. Kang, J. Melançon, A.D. Pelton, C. Robelin, and S. Petersen, *Calphad* 33, 295 https://doi.org/10.1016/j.calphad.2008.09.009 (2009).
34. C.W. Bale, E. Bélisle, P. Chartrand, S.A. Decterov, G. Eriksson, A.E. Gheribi, K. Hack, I.H. Jung, Y.B. Kang, J. Melançon, A.D. Pelton, S. Petersen, C. Robelin, J. Sangster, P. Spencer, and M.A. Van Ende, *Calphad* 55, 1 https://doi.org/10.1016/j.calphad.2016.07.004 (2016).
35. T.W. Liang Jiang, and L. Ma, *Bull. Chin. Ceram. Soc.* 37, 4034 (**in Chinese**) (2018).
36. Z. Deng, University of Science and Technology Beijing, 2015. (**in Chinese**).
37. T.W. Liang Jiang and J. Li, *Mater. Rep.* 33, 2490 (**in Chinese**) (2019).
38. J. Li, Yu. Qijun, and J. Wei, *J. Wuhan Univ. Technol.* 34, 19 (**in Chinese**) (2012).
39. Y. Luo, University of Science and Technology Beijing, 2023. (**in Chinese**).